Electronic Supplementary Information

Overcoming the problem of insolubility to controllably synthesize AuCo alloy as high performance electrocatalyst for oxygen reduction reaction

Zhandong Ren,[a] Zhiqiang Xie,[a] Ruoxi Ming,[a] Yiping Zhan,[a] Yuefei Xin,[a] Juanjuan Han,[a] Lin Zhuang,[b] Yi Liu[c] and Yuchan Zhu*[a]

a. School of Chemical and Environmental Engineering, Wuhan Polytechnic University, Wuhan, 430023, P. R. China.

b. College of Chemistry and Molecular Sciences, Hubei Key Lab of Electrochemical Power Sources, Wuhan University, Wuhan, 430072, PR China.

c. State Key Laboratory of Separation Membranes and Membrane Processes, School of Chemistry, Tiangong University, Tianjin 300387, P. R. China.

* Corresponding author:

Experimental methods

Preparation of Au/C/Ti, AuCo alloy/C/Ti and Pt/C/Ti

5 mg of XC-72 carbon powder was dispersed into 1 mL 0.05 wt% Nafion/ethanol solution, and the ultrasonic dispersion was carried out for 30 min to obtain carbon powder ink. Then, C powder ink was evenly dripped on the treated Ti foil (cleaned by acetone, water and ethanol) to form a C/Ti matrix. Then the C/Ti matrix was transferred into a vacuum chamber. Using 99.99% Au disk and 99.99% Co disk as sputtering targets, AuCo alloy/C/Ti electrodes were prepared in high vacuum magnetron sputtering instrument (TRP-450, SKY Technology Development, China). Before sputtering, the vacuum chamber was evacuated to 5×10^{-4} Pa, and then high purity argon was introduced to adjust the pressure of the vacuum chamber to 1.0 Pa. Au target was controlled by common magnetic field, while Co target was controlled by strong magnetic field. Different proportions of AuCo alloy/C/Ti electrodes are obtained by controlling DC power supply as shown in Table 1 (ESI†). The sputtering power of Au target is fixed at 10 W, and the sputtering power of Co target is reduced from 100 to 10 W, thus obtaining $Au_{30}Co_{70}$, $Au_{37}Co_{63}$, $Au_{46}Co_{54}$, $Au_{59}Co_{41}$, $Au_{78}Co_{22}$ and $Au_{87}Co_{13}$ alloys respectively. The magnetron sputtering preparation of Au/C/Ti is the same as that of AuCo alloy/C/Ti, except that Au target is used alone for sputtering. When preparing Pt/C/Ti by magnetron sputtering, Pt target (99.99%) was used instead.

Materials characterization

X-ray diffraction (XRD) patterns were acquired on an XRD-7000 X-ray diffractometer (Shimadzu, Japan). Transmission Electron Microscopy (TEM) were conducted on an JEM-2100F (JEOL, Japan). Scanning Electron Microscope (SEM) images were taken with a ΣIGMA field-emission SEM (Zeiss, Germany). X-ray photoelectron spectrometry (XPS: ESCLAB 250Xi, Thermo Fisher Scientific, The United States) with monochromatized Al Ka radiation was used to analyze the electronic properties. Analysis of the composition of the electrode was carried out by X-ray fluorescence (XRF: EDX-7000, Shimadzu, Japan).

Electrochemical measurements

The electrochemical experiments were carried out in a typical three-electrode electrochemical cell with a carbon paper as a counter electrode (TGP-H-090, Toray, Japan) and Hg/HgO/KOH (1.0 M) as the reference electrode (R0501, Tianjin Aida Hengsheng Technology Development Co., Ltd, China). The preparation process of working electrode is as follows. 50 wt% AuCo/C (Au/C, Pt/C) was ultrasonically removed from the Ti foil to the ethanol solution to obtain a catalyst-ethanol dispersion solution. Next, 50 wt% AuCo/C (Au/C, Pt/C) power sample was obtained by vacuum drying at 40 ℃ for 12 h. Then, 5 mg of AuCo/C (Au/C, Pt/C) power was dispersed into 1 mL 0.05 wt% Nafion/ethanol solution, and the ultrasonic dispersion was carried out for 30 min to obtain catalyst ink. 20 μL catalyst ink were dropped on a glassy carbon electrode with a diameter of 5 mm, and the working electrode was obtained after drying. The loading of AuCo (Au, Pt) is 0.255 mg cm^{-2}. Cyclic voltammetry (CV) measurements were performed in Ar-saturated 1.0 M KOH solution at the scan rate of 100 mV s^{-1}. The electrochemical surface areas (ECSAs) were calculated by scanning the double layer (0.2-0.3 V vs. RHE) at different scanning speeds (5, 10, 15, 20, 30, 40, 50, 60, 70, 80, 90, 100 mV s^{-1}). The oxygen reduction reaction (ORR) polarization curves were obtained by sweeping at a scan rate of 5 mV s^{-1} with the different rotation rate (100, 400, 900, 1600, 2500rpm) in O_2-saturated 1.0 M KOH. The following equations (Koutecky-Levich, KL) were used

for the calculation of the kinetic current and electron transfer number (n).

$$j^{-1} = j_k^{-1} + j_d^{-1} = j_k^{-1} + (B\omega^{1/2})^{-1}$$

$$B = 0.62nFC_0D_0^{2/3}v^{-1/6}$$

where j is the actual current density, j_k and j_d are the kinetic- and diffusion-limiting current densities, respectively, B is the slope, ω is the angular velocity of rotating disk electrode system (RDE, MSR, Pine, The United States), n is the electron transfer number, F is the Faraday constant (96485 C mol^{-1}), C_0 is the bulk concentration of O_2 (0.84×10^{-6} mol cm^{-3}), D_0 denotes the diffusion coeffcient of O_2 (1.85×10^{-5} cm^2 s^{-1}), and v represents the kinetic viscosity of the electrolyte (0.0106 cm^2 s^{-1}) in 1.0 M KOH aqueous solution. To investigate the durability of catalyst, the accelerated durability test (AST) is carried out in the O_2-saturated 1.0 M KOH for 10,000 cycles between 0.6 and 1.1 V at 100 mV s^{-1}.

DFT calculations

First-principles calculations were performed using the Vienna Ab Initio Simulation Package (VASP, version 5.3) within a PBE (Perdew Burke Ernzerhof) generalized gradient approximation (GGA) to the exchange and correlation functional. A projector augmented wave (PAW) basis along with a plane-wave kinetic energy cutoff of 450 eV was employed for all computations. During the geometry optimization, the adsorbate layer and the top three layers of the slab were allowed to relax. The energies were converged to 1×10^{-3} eV per atom and ionic relaxations were allowed until the absolute value of force on each atom was below 0.02 eV/A. $AE_O = E(O/M) - E(M) - 1/2E(O_2)$, such that the negative value indicates the dissociation of O_2 on the studied surface being thermodynamically spontaneous, whereas the positive means the opposite. The free energies of ORR intermediates are defined as $\Delta G = \Delta E + \Delta ZPE - T\Delta S$, where ΔE, ΔZPE, T, and ΔS represent the reaction energy, zero-point energy, temperature (298.15 K), and the entropy, respectively.

The overall reaction scheme of the ORR can be written as:

$$* + O_2(g) + H_2O(l) + e^- \rightarrow OH^- + *OOH$$

$$*OOH + e^- \rightarrow OH^- + *O$$

$$*O + H_2O(l) + e^- \rightarrow OH^- + *OH$$

$$*OH + e^- \rightarrow OH^- + *$$

where * represents the catalyst surface and *OOH, *O and *OH species are oxygenated intermediates.

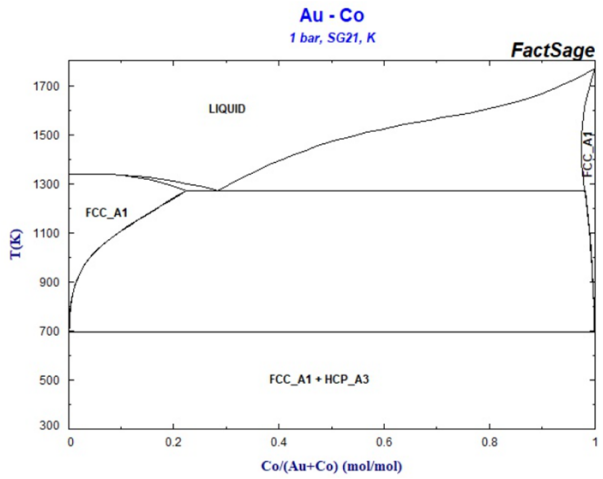

Figure S1 Au-Co Phase Diagrams in the SGTE - SGTE 2022 Alloy Phase Diagrams. (https://www.crct.polymtl.ca/FACT/phase_diagram.php?file=Au-Co.jpg&dir=SGTE2022)

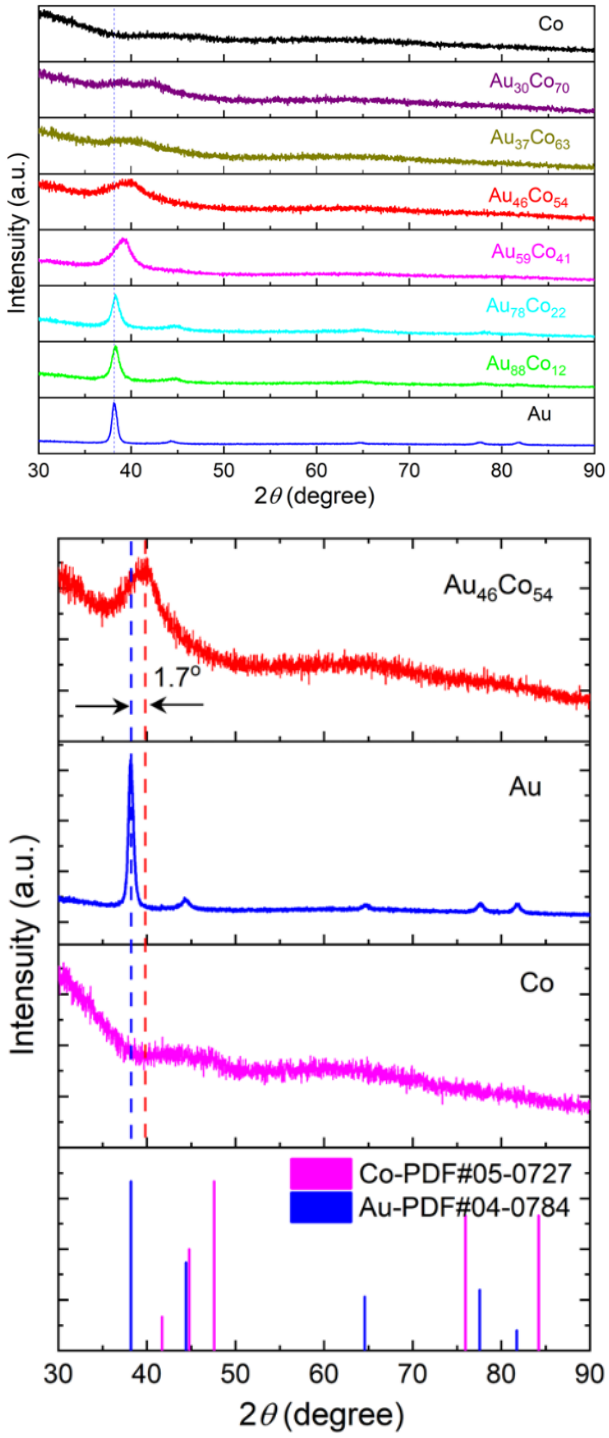

Figure S2 X-ray diffraction patterns of Au, Co and AuCo alloys with different proportions.

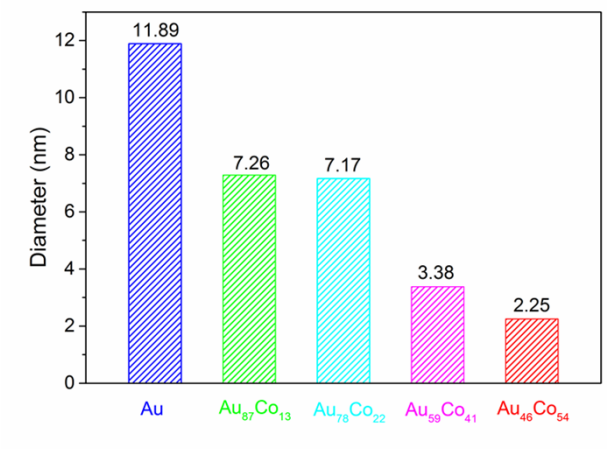

Figure S3 Particle sizes of AuCo alloys with different proportions.

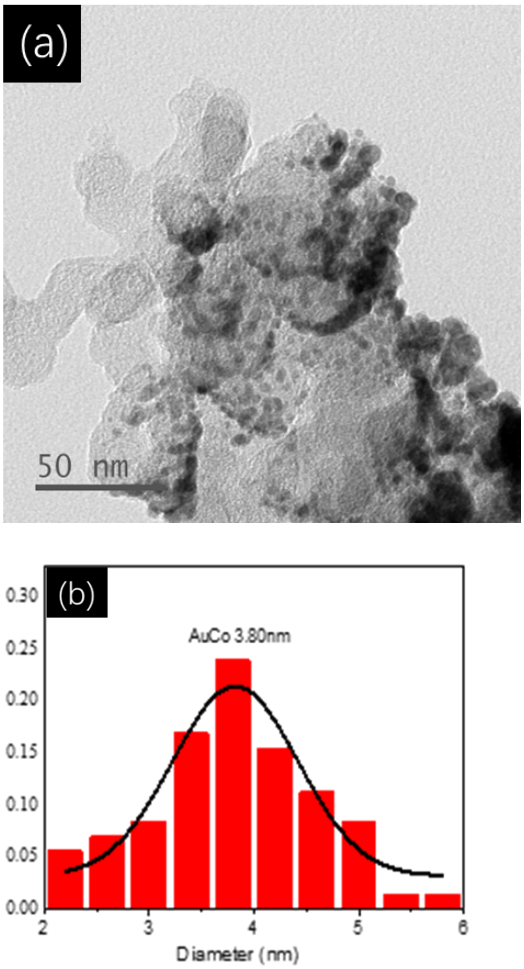

Figure S4 TEM image with the particle size distribution of $Au_{46}Co_{54}$ alloy.

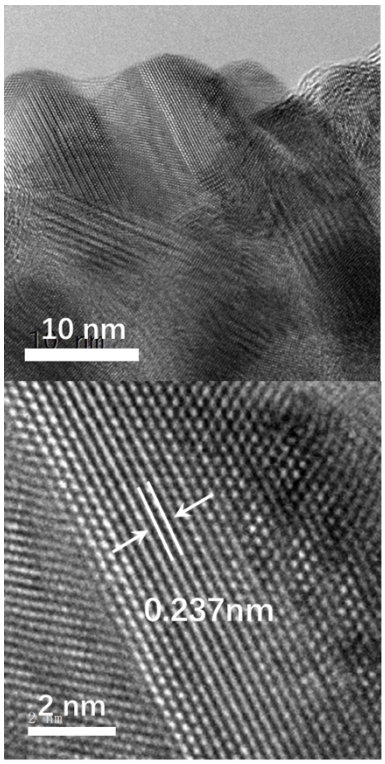

Figure S5 HRTEM images of Au.

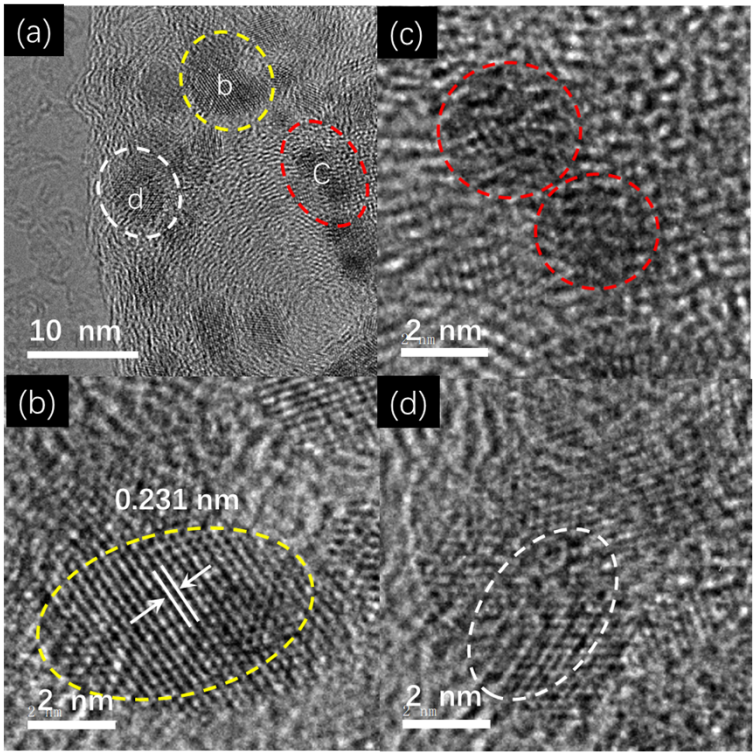

Figure S6 HRTEM images of $Au_{46}Co_{54}$ alloy.

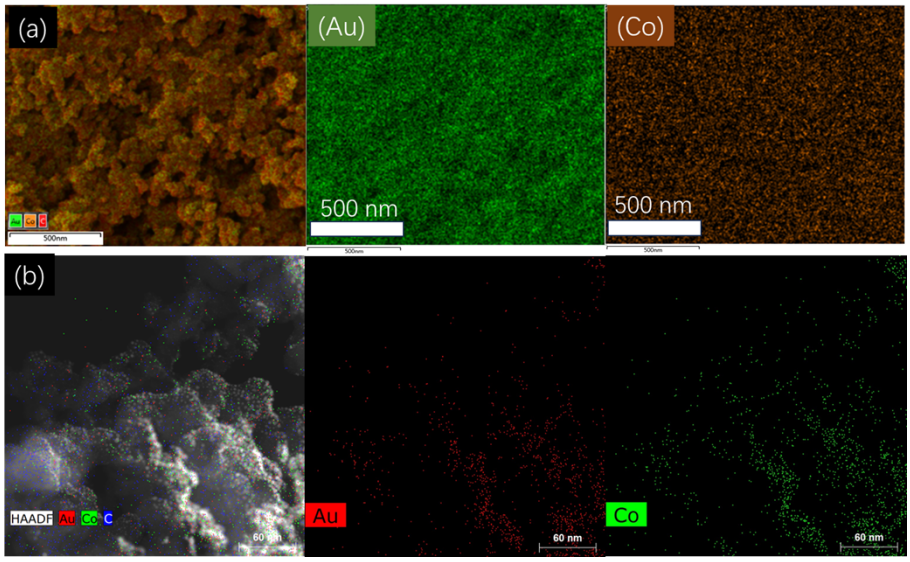

Figure S7 The SEM-EDS (a) and HAAD-STEM-EDS (b) mappings of $Au_{46}Co_{54}$ alloy.

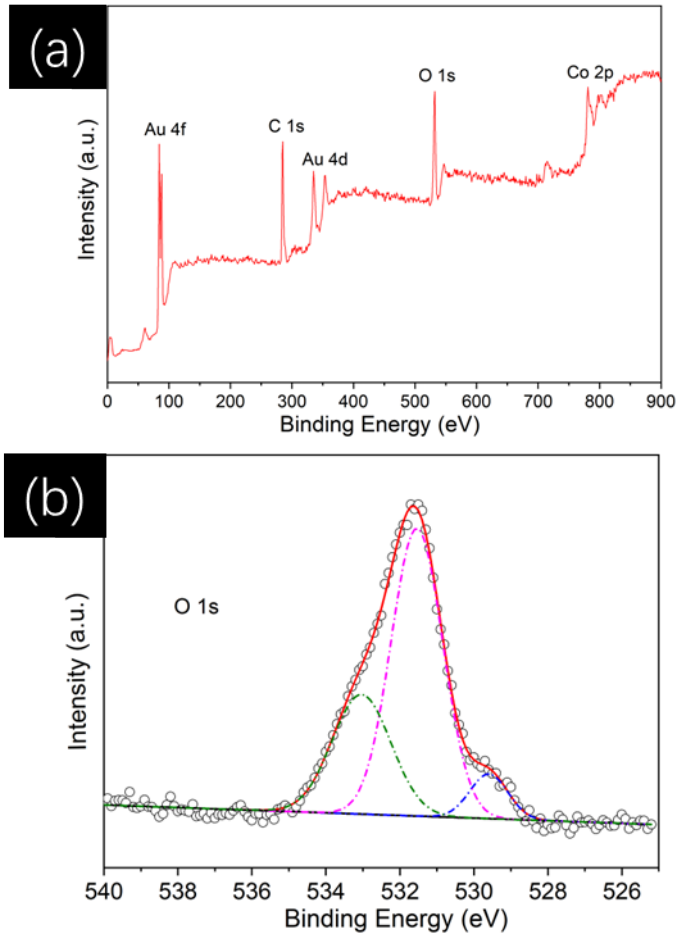

Figure S8 The survey (a) and core-level spectra of O 1s (b) of $Au_{46}Co_{54}$ alloy.

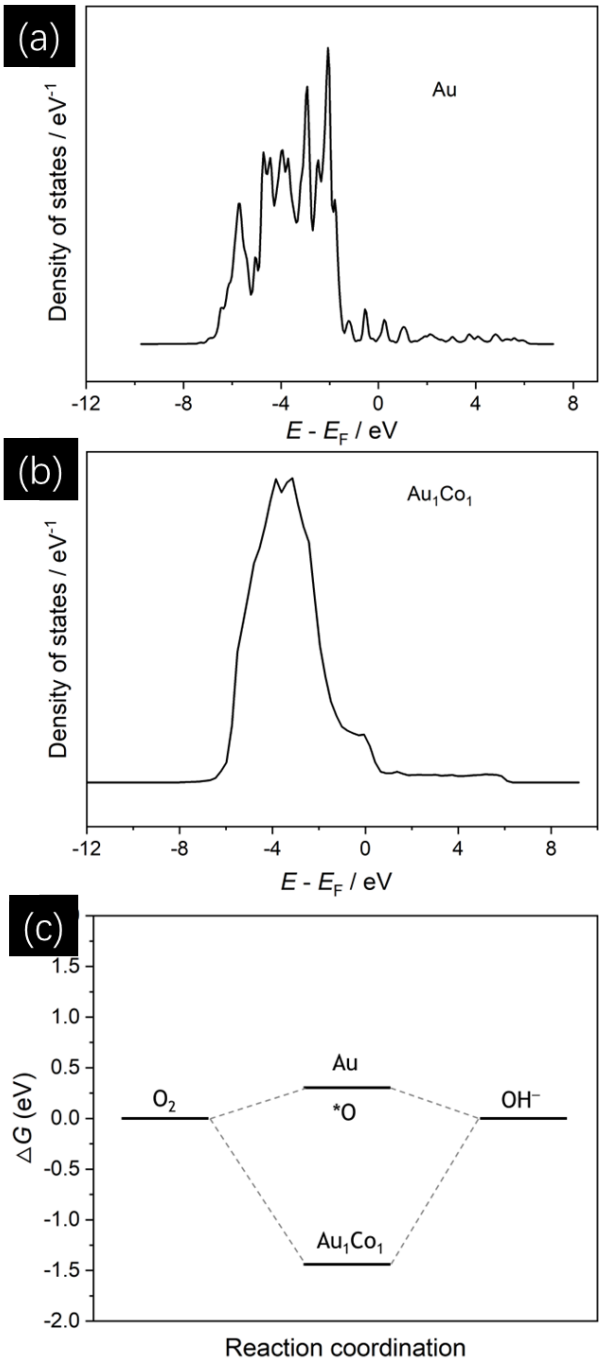

Figure S9 The density of states (DOS) of Au (a) and Au_1Co_1 (b) and ΔG (c) of Au and Au_1Co_1 (U = 1.23 V).

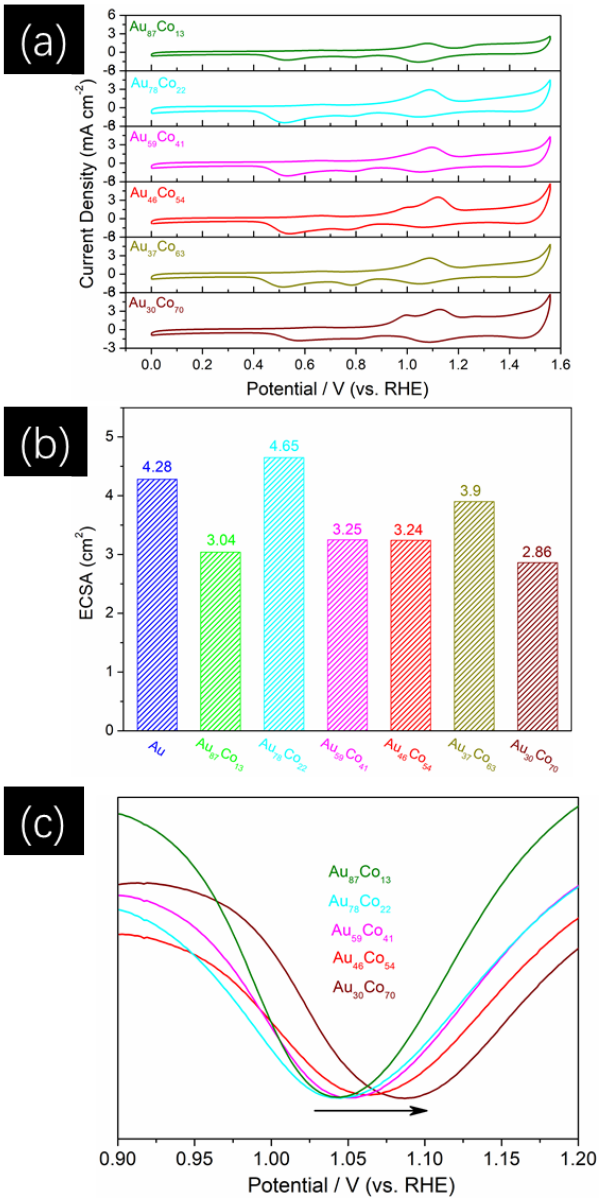

Figure S10 CVs (a), ECSAs (b) and oxygen reduction peaks (c) of AuCo alloys with different proportions.

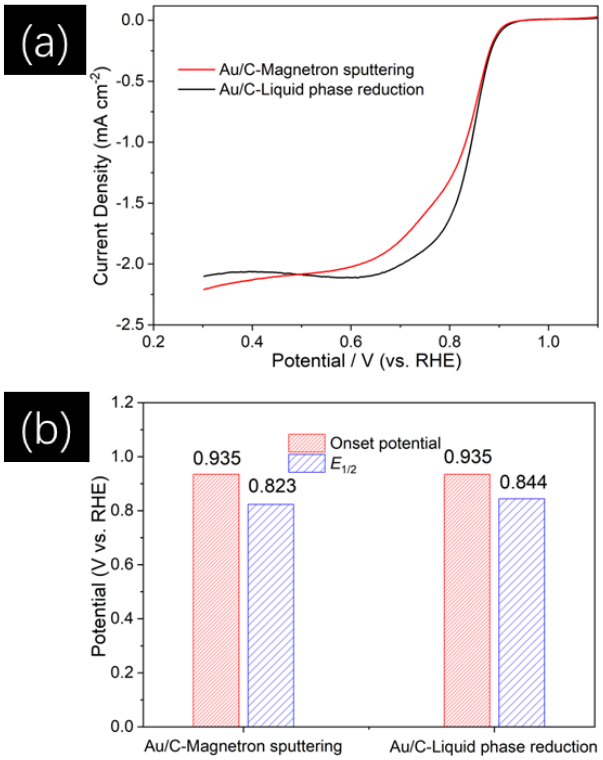

Figure S11 ORR activities (a), E_{onset} and $E_{1/2}$ (b) of Au-Magnetron sputtering and Au-Liquid phase reduction.

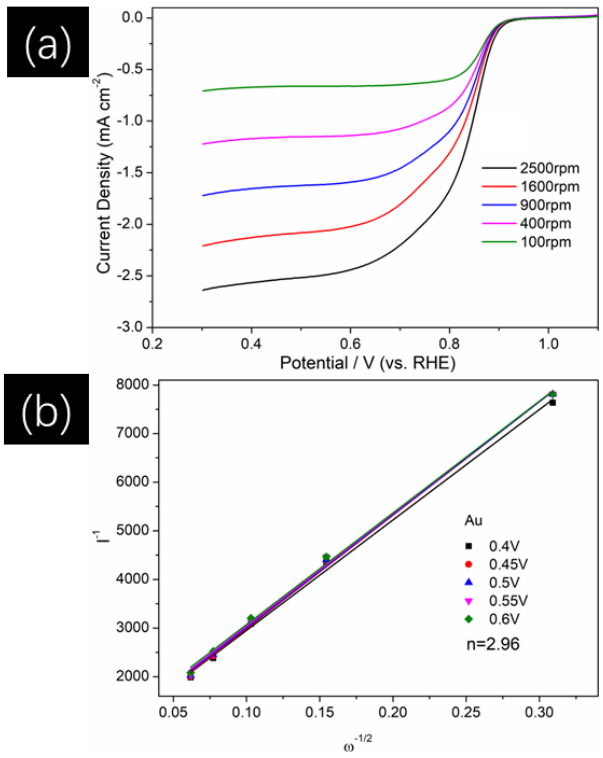

Figure S12 ORR activities at different rotate speeds (a) and transfer electron number (n) under different potential (b) of Au-Magnetron sputtering.

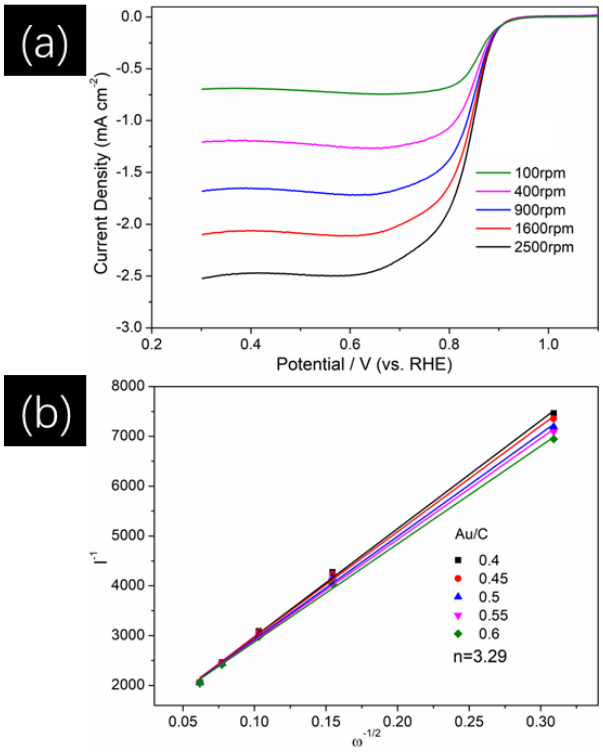

Figure S13 ORR activities at different rotate speeds (a) and transfer electron number (n) under different potential (b) of Au-Liquid phase reduction.

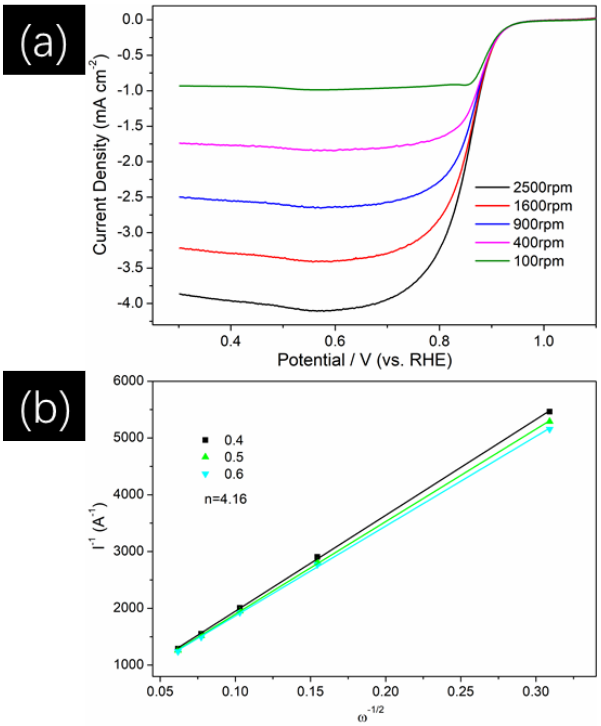

Figure S14 ORR activities at different rotate speeds (a) and transfer electron number (n) under different potential (b) of $Au_{46}Co_{54}$.

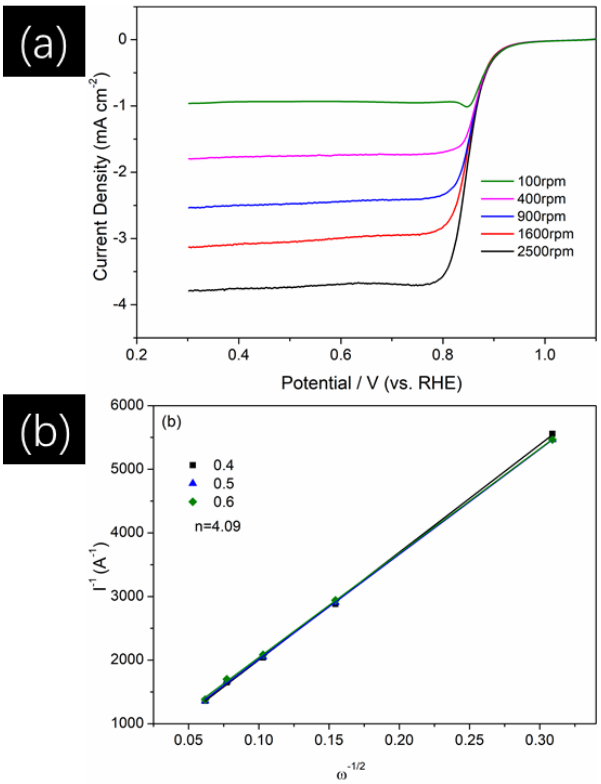

Figure S15 ORR activities at different rotate speeds (a) and transfer electron number (n) under different potential (b) of Pt.

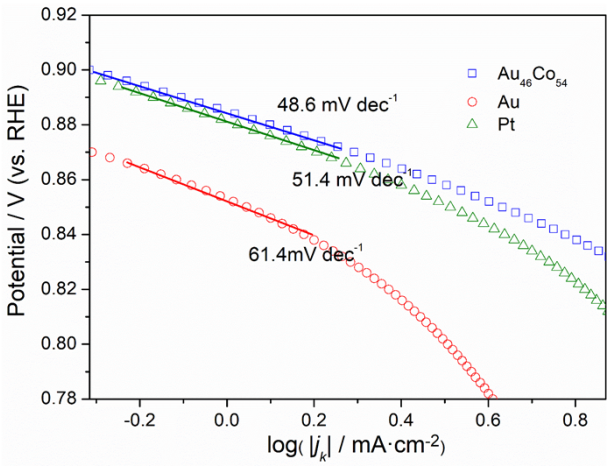

Figure S16 Tafel slopes of Au, $Au_{46}Co_{54}$ and Pt.

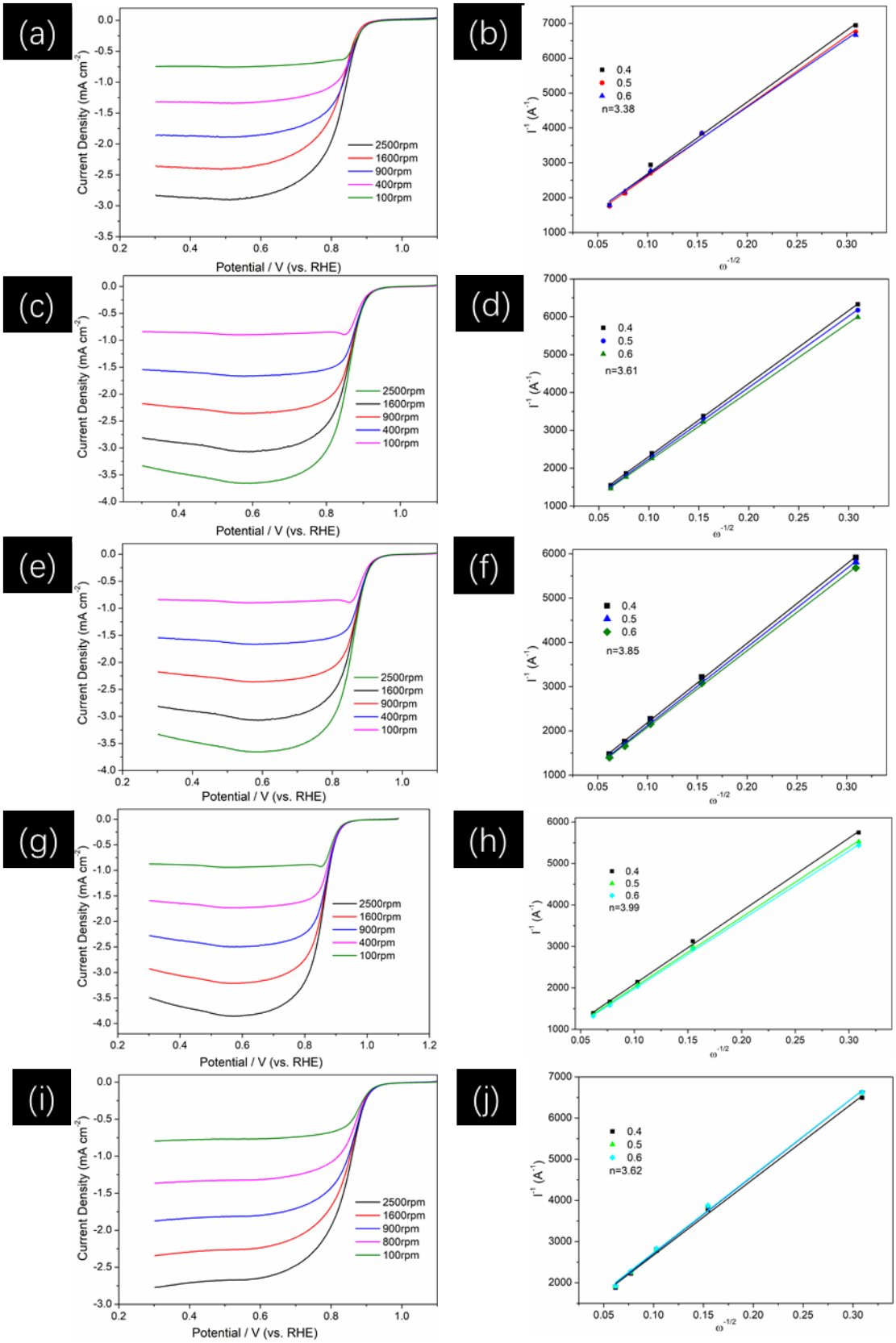

Figure S17 ORR activities at different rotate speeds (a) and transfer electron number (n) under different potential (b) of AuCo alloys with different ratios.

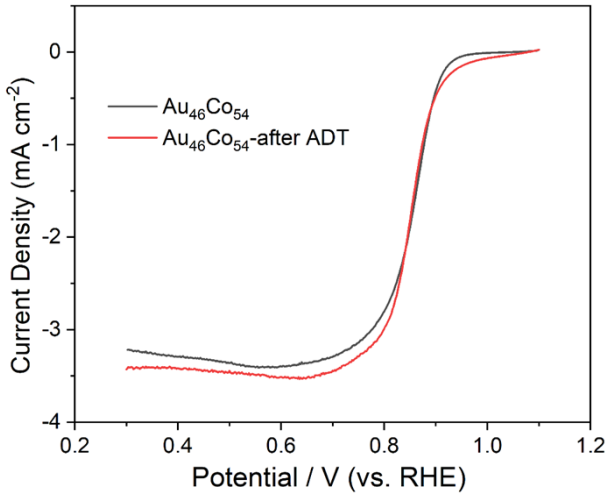

Figure S18 The ORR stability test for $Au_{46}Co_{54}$ with the RDE (rotating disk electrode) potential cycling from 0.6 to 1.1 V (10,000 cycles) at a scan rate of 100 mV s^{-1} in O_2-saturated 1.0 M KOH.

Table S1 Composition analysis of AuCo alloy electrodes with different sputtering power by XRF

Catalyst	Sputtering power / W		Content / mol%	
	Au	Co	Au	Co
$Au_{30}Co_{70}$	10	100	30	70
$Au_{37}Co_{63}$	10	80	37	63
$Au_{46}Co_{54}$	10	60	46	54
$Au_{59}Co_{41}$	10	40	59	41
$Au_{78}Co_{22}$	10	20	78	22
$Au_{87}Co_{13}$	10	10	87	13

Table S2. Comparison of the ORR activity of the optimized AuCo alloy with other Au-nonprecious metal alloy electrocatalysts in the alkaline solution.

Catalyst	E_{onset}	$E_{1/2}$ (V)	$\Delta E_{1/2}$ (mV)	SA mA/cm^2	Measured at (V)	Ref.
AuCo	**0.967**	**0.862**	**12**	**0.87**	**0.80**	**This work**
pure Au	**0.935**	**0.823**	**-27**	**0.14**	**0.80**	
AuNi NDs	1.032	0.911	81	0.46	0.85	Adv. Funct. Mater., 2017, 27, 1700260
AuCu NF	0.960	0.848	18	0.40	0.85	
Pure Au NPs	0.886	0.790	-40	---	---	
Dealloyed AuNi	1.030	0.896	67	0.50	0.80	J. Mater. Chem. A, 2016, 4, 17828
AuNi	1.000	0.869	40	0.43	0.80	
pure Au	0.900	0.810	-19	0.15	0.80	
Dealloyed AuNi	---	0.884	40	0.59	0.80	Adv. Funct. Mater., 2016, 26, 1590
AuNi	---	0.824	-20	0.29	0.80	
$AuCu_3$ NP	---	0.820	-10	---	0.80	Small, 2014, 10, 2662–2669
AuCu NP	---	0.800	-30	---	0.70	
AuCu NP	---	---	---	0.28	0.85	J. Mater. Chem., 2012, 22, 15769–15774
AuNi-Cu_2O	0.910	0.820	---	---	---	Electrochim. Acta 2018, 283, 1411
$AuAg_{3.2}$ NS	1.004	0.858	32	1.36	0.85	ACS Appl. Mater. Interfaces 2018, 10, 6276
AuAg Janus NP	0.917	---	---	---	0.68	Langmuir, 2012, 28, 17143
AuAg NP	0.920	---	---	---	0.85	Nanoscale, 2015, 7, 9627
Ag@Au SNP	0.950	---	---	---	0.66	Nanoscale, 2016, 8, 14565
Au@Ag NP	0.910	---	---	---	0.66	
Ag@Au NP	0.770	---	---	---	0.66	
Au(100)	0.960	0.800	---	---	---	Mater. Chem. Phys., 1989, 22, 349.
Au(110)	0.840	0.700	---	---	---	ACS Catal., 2015, 5, 4643.
Au(111)	0.840	0.670	---	---	---	

(a) E_{onset}, onset potential; $E_{1/2}$, half-wave potential; $\Delta E_{1/2}$, the difference of half-wave potential ($E_{1/2}$) between the reported catalyst and the commercial Pt/C, the positive value represents the improvement in $E_{1/2}$ with respect to Pt/C, the minus value represents the opposite trend; SA, specific activity.

(b) Abbreviations: ND, nanodendrites; NF, nano film; NP, nanoparticles; NS, nanosponges; SNP, semishell nanoparticle.